Theoretical Investigation of Compact Intersections of Silicon Slot Waveguides

Kyoung-Soo Kim

Department of Electrical Engineering

Graduate School of UNIST

Theoretical Investigation of Compact Intersections of Silicon Slot Waveguides

A thesis
submitted to the Graduate School of UNIST
in partial fulfillment of the
requirements for the degree of
Master of Science

Kyoung-Soo Kim

12. 30. 2016 of submission
Approved by

Advisor
Min-Suk Kwon

Theoretical Investigation of Compact Intersections of Silicon Slot Waveguides

Kyoung-Soo Kim

This certifies that the thesis of Kyoung-Soo Kim is approved.

12. 30. 2016 of submission

Signature

Advisor: Min-Suk Kwon

Signature

Jingook Kim: Thesis Committee Member #1

Signature

Jongwon Lee: Thesis Committee Member #2

Contents

List of Figures

Figure 3-10. A schematic diagram of blunt corners of slot region in taper structures.

Figure 3-11. Fig. 3-11. (a) The throughput depending on blunt radius. (b) The crosstalk and reflection depending on blunt radius. The Black line is depicted crosstalk and red dot line shows reflection.

Figure 3-12. Throughput, Crosstalk and Reflection depending on wavelength in the range from 1.45μm to 1.65μm.

Nomenclature

MMI	Multi-mode interference
MMW	Multi-mode waveguide
TE	Transverse-electric
SEM	Scanning electron microscope
CMOS	Complementary metal-oxide-semiconductor
SOI	Silicon on insulator
FCA	Free carrier absorption

Abstract

Optical interconnection is considered as an alternative solution to electrical interconnection since the former can overcome limits of the latter. Low power consumption and high-speed data transmission are expected from optical interconnection. Matrix switches are an important element of optical interconnection, and conventional on-chip matrix switches are based on silicon strip waveguides. Since such switches are controlled by using the plasma dispersion effect, there are a few disadvantages such as the loss concomitant with the effect and limited switching speed. The disadvantages may be removed if on-chip matrix switches are constructed from silicon slot waveguides with electro-optic polymer filling their slots. This is because the electro-optic effect has better tuning properties than the plasma dispersion effect. For matrix switches based on silicon slot waveguides, intersections of silicon slot waveguides must be developed. This research theoretically investigates compact efficient intersections of silicon slot waveguides. The proposed intersection consists of mode transformers between slot waveguides and multimode strip waveguides, which are connected to a crossing of the multimode waveguides. In the mode transformer, the rails of the slot waveguide are linearly tapered to be connected to the multimode strip waveguide, and the slot is terminated within the tapering region. The mode transformer converts the slot waveguide mode into even transverse-electric (TE) modes. Because of multimode interference among the even TE modes in the crossing, the intersection can work efficiently. How to design the intersection is explained. The throughput, crosstalk, and reflectance of the intersection are –0.078 dB, –41 dB and –36 dB, respectively, at a wavelength of 1.55 μm. In the wavelength interval between 1.5 μm and 1.6 μm, the throughput is larger than –0.17 dB, the crosstalk is smaller than –40 dB, and the reflectance is smaller than –29 dB. The performance of the intersection is better than those of previous intersections of silicon slot waveguides. The footprint is 79.2 μm^2, which is just less than 33 % of those of previous intersections. Finally, the fabrication tolerance of the intersection is discussed. It is demonstrated that the intersection is quite tolerable to fabrication errors.

1. Introduction

1-1. Optical interconnection based on silicon photonics

Optical communication is focused as alternative technology for electrical communication. Electrical wires have fundamental limitations of power consumption, a carrier frequency, and complexity of integration. Optics can overcome those limitations. Relative long distance lines can be realized due to no resistive loss of wires. Optical communication can be operated with high frequency. Moreover optics allows wavelength-division multiplexing that is impossible in single electrical wire line. For densely integrated circuit, optics can overcome problems of electrical interconnects. Due to transparency of silicon in telecommunication wavelength region, 1550nm, silicon can be used for waveguide core. A high refractive index of silicon make light highly confined in waveguide. Moreover, silicon photonics is compatible with CMOS fabrication process for mass production [1].

1-2. Intersections of silicon waveguides

Waveguide intersection is essential component for photonics integrated circuit. Among that waveguide intersections are indispensable elements for a resonator based switching component. For conventional waveguide intersection, relatively large lateral components in intersection center deteriorate insertion loss and crosstalk. A conventional silicon waveguide intersection shows experimental performance as for insertion loss over -1dB and crosstalk about -10dB[6]. A Resonant-cavity based intersection was proposed to resolve degradation of insertion loss and crosstalk. But it is inappropriate to broadband operation. Due to that problems, multi-mode interference based intersection is utilized to achieve better intersection performance[7]. Modes with different effective indices propagate with interference each other. The Gaussian-like lateral confined beam at the intersection center restrains distortion from radiation and diffraction by suppressing lateral components. The confined light feels less optical variation when propagates through intersection. Fig. 1-1. is a example of silicon waveguide intersection based on multi-mode interference[2]. As shown in figure, light propagates to through port efficiently with small distortion component and throughput is small, -0.12dB.

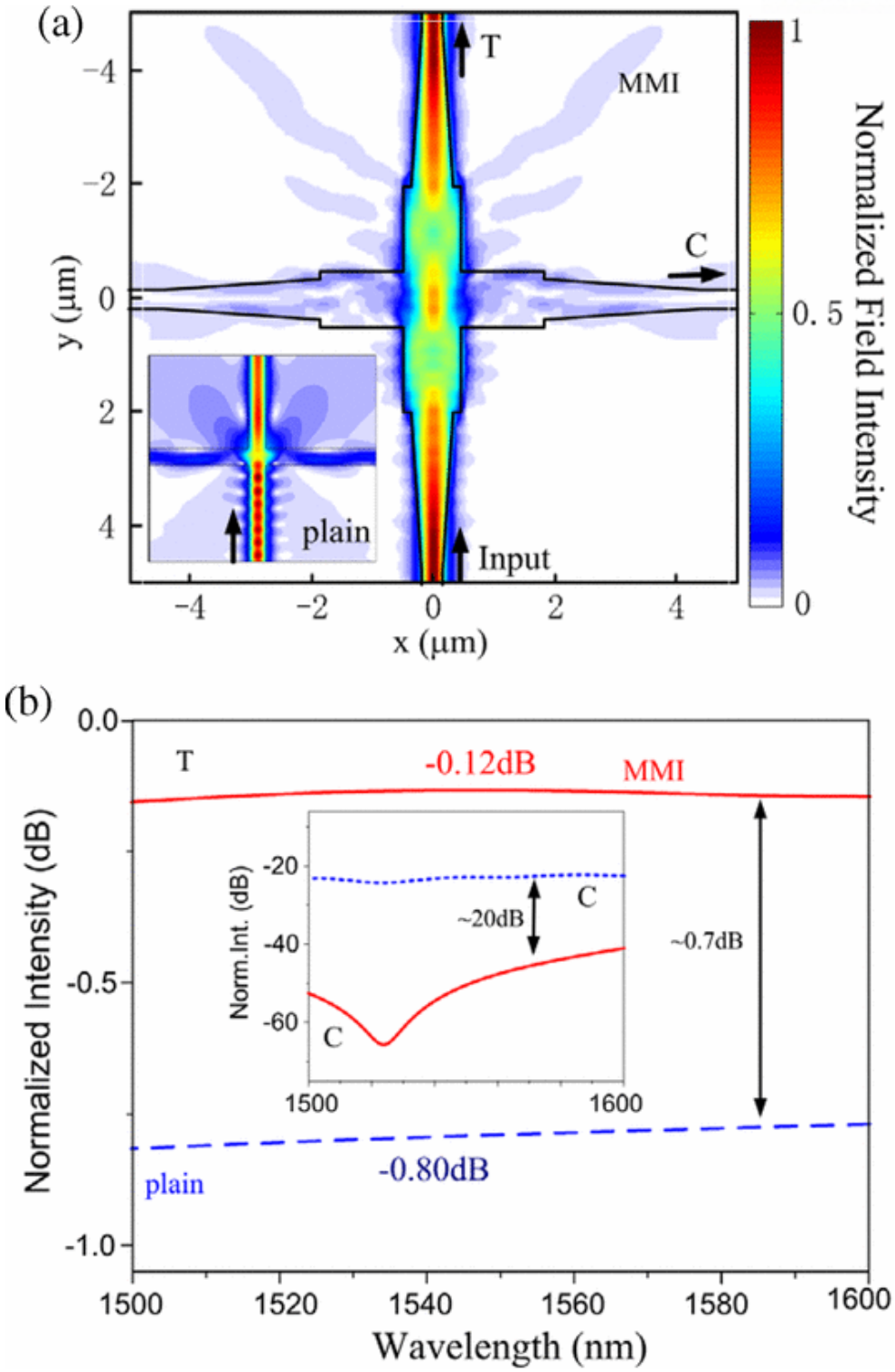

Fig. 1-1. Example of Silicon waveguide intersection based on multi-mode interference (MMI)[2].

Furthermore intersection structure is essential components to compose optical switch matrix. Fig. 1-2. depicts switching mechanism using a micro-ring resonator.

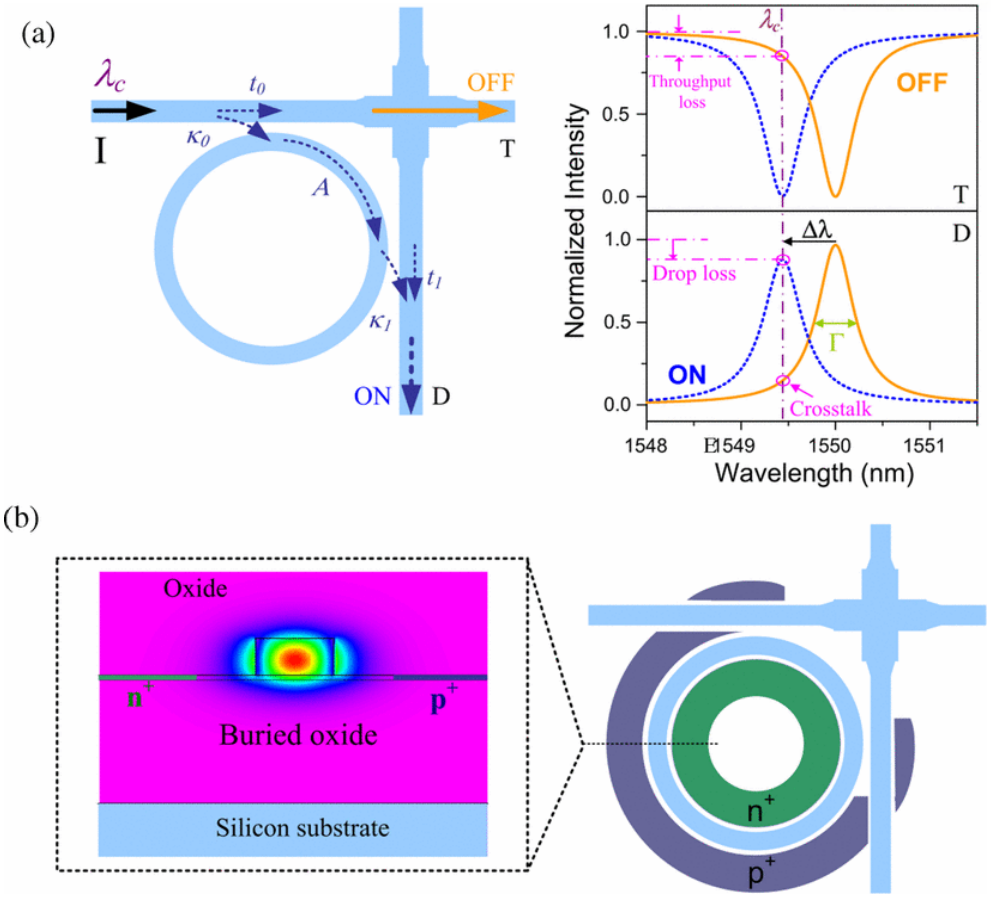

Fig. 1-2. Example of switch matrix based on multi-mode interference intersection[2].

By applying electrical signal bring carrier accumulation then change the refractive index. Changed resonance frequency of ring resonator results to change direction of light. However carrier injection type switches based on micro-ring resonator has switching speed limitation. Fundamentally limited transient time causes switching time limitation [2].

1-3. Intersections of silicon slot waveguides

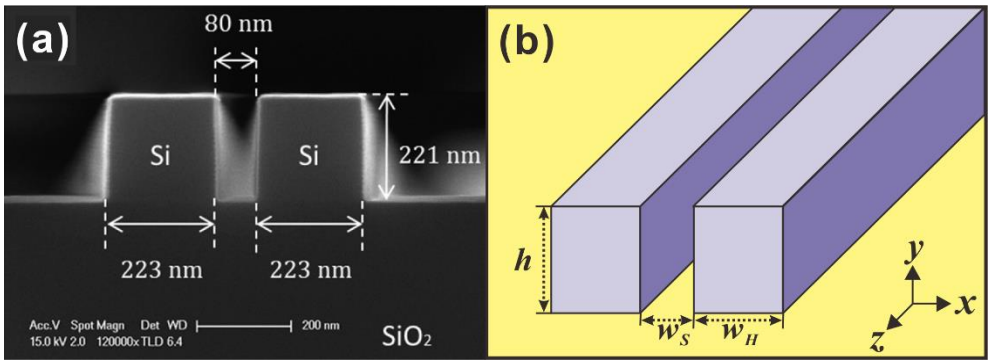

Fig. 1-3. (a) An example of fabricated slot waveguide structure[8] (b) A schematic of slot waveguide.

Slot waveguide is recently attended for unique properties of highly confining electric field in small area[8]. By placing electro-optic polymer in high confined area, a large electro-optic effect can be achieved. Most of all, electro-optic polymer can overcome a switching speed limitation of carrier injection type switch. A slot waveguide is composed of two high index silicon cores. Fig. 1-2. (a) is a SEM image of fabricated slot waveguide[9]. We referred sizes of slot waveguide. Proposed intersection structure is based on slot waveguide shown in Fig. 1-2. (b). The height of silicon core, *h*, is 250nm and the width of silicon core, w_H, is 220nm. The distance between two rails is defined by gap width, w_S, is 100nm consistently along longitudinal direction.

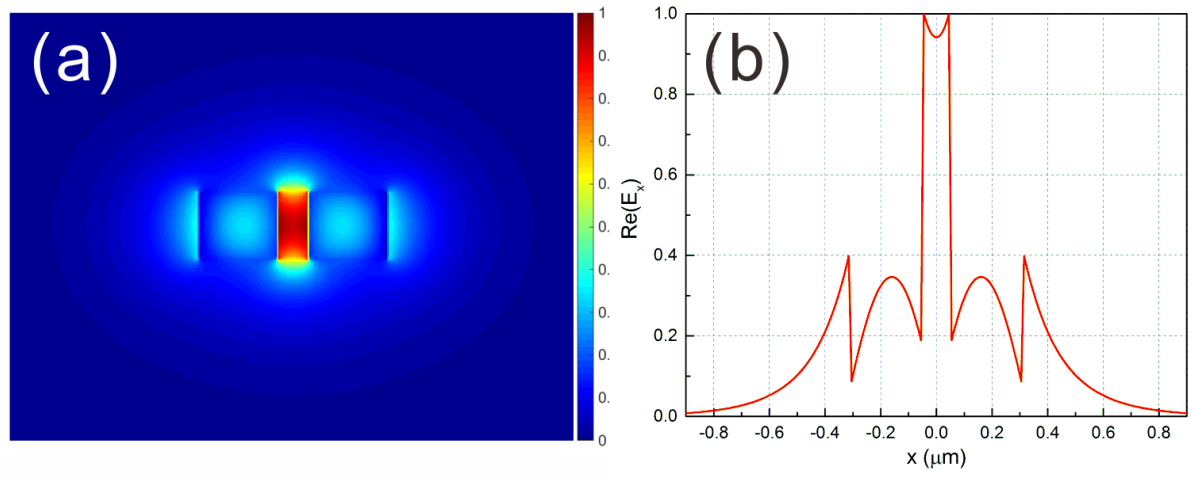

Fig.1-4. (a) Normalized electric field distribution, *Ex*, of slot waveguide TE_0 mode (b) The real part of the normalized electric field versus horizontal position, x, in the middle height of rails.

The mode profile of slot waveguide TE_0 mode is shown in Fig. 1-4. (a). The normalized transverse electric field, *Ex*, is highly confined in slot region between two rails. Highly confined electric field in

low-index region between two high-index cores is induced due to high-index contrast. Large electric field discontinuity from high-index contrast makes strong confined electric field in the gap region. That strong filed is applied for a variety of application such as optical modulators[10], multi-mode interference splitters[11], micro-ring resonators[12], and sensors[13]. By placing electro-optic polymer in gap region, efficient and fast modulation is possible[10]. Furthermore slot waveguide facilitates efficient and fast switch matrix. Some designs are reported for slot waveguide intersections. Recently reported designs of intersection of slot waveguide are depicted on Fig. 1-4 and 1-5.

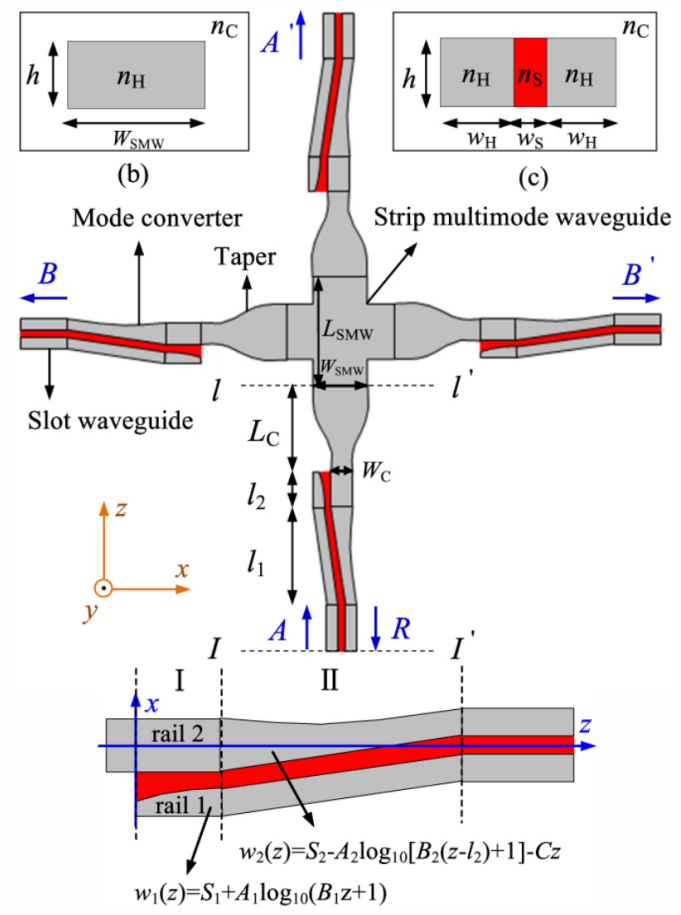

Fig. 1-5. A design of silicon slot waveguide intersection [4].

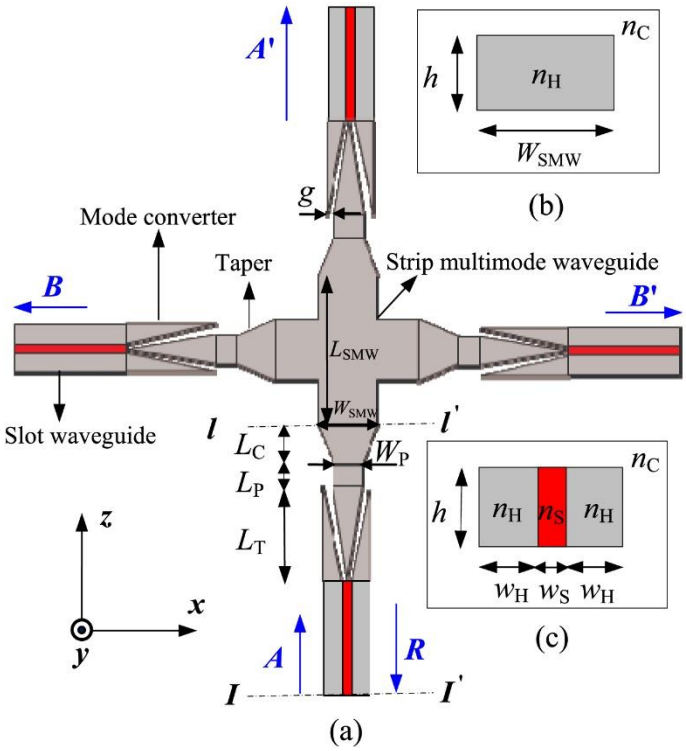

Fig. 1-6. A design of silicon slot waveguide intersection [5].

For a simple abrupt junction between a slot and a strip waveguide, large coupling loss occurs due to large mode mismatch. For that reason, mode converters are adapted in transition region between a slot and a strip waveguide. The design in Fig. 1-4. is based on logarithmical mode converter to convert slot waveguide mode to strip waveguide mode efficiently. The device throughput, crosstalk and reflection is -0.131dB, -37.44dB and -35.47dB. A total size of design is 432.6 μm^2[4]. The structure shown in Fig. 1-5. is utilizing linearly taper converter. That device throughput, crosstalk and reflection is -0.086dB, -35.58dB and -27.51dB, respectively. A dimension of structure is 246.5μm^2[5]. But transition region in these structure is composed with mode converter and taper. It has relatively large size owing to using mode converter and taper size both.

2. Structure and analysis method

2-1. Structure

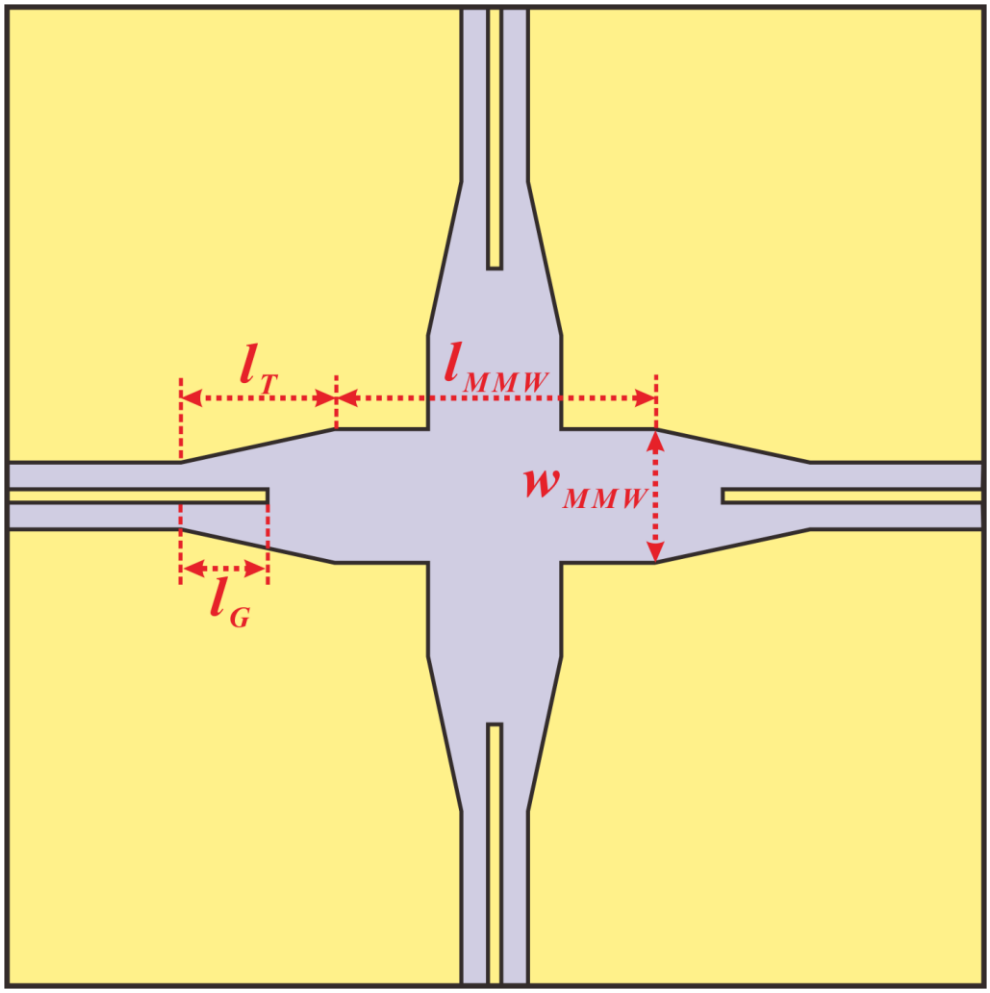

Fig. 2-1. Proposed structure of silicon slot waveguide intersection.

A fundamental TE_0 mode in the slot waveguide converts to higher order modes in multi-mode waveguide, including TE_4 mode, through taper region. In the multi-mode waveguide, some lateral symmetric TE modes, TE_0, TE_2 and TE_4, are dominantly excited. These modes propagate with interference each other. At specific moderate position in propagation direction, an intersection center, a narrow Gaussian-like beam profile can be obtained. The lateral confined beam goes through intersection with small distortion. After then, modes in multi-mode waveguide converts to output slot waveguide TE_0 mode through taper structure same as input taper. As a result, high throughput and small crosstalk intersection structure can be achieved. The device is based on SOI platform. A cladding material is SiO_2 with 3μm thickness both upper and down sides. A thickness of silicon waveguide is 250nm and slot gap

width is 100nm consistently along slot waveguide. A taper length, l_T, is 3000nm long to reduce loss from conversion to higher order modes in taper region. A MMW length, l_{MMW}, is chosen as 2900nm to highly lateral confine light at the intersection center for efficient intersection. A MMW width, w_{MMW}, is 1700nm to excite TE_0, TE_2 and TE_4 mode in MMW region. In taper region wider MMW width makes reduce transition loss when slot TE mode converse to higher modes in MMW region. A key parameter is gap region length, l_G, which is engineered to improve performance and reduce device size. Recent researches are limited relatively narrow MMW width as 1200nm to excite only two symmetric modes, TE_0 and TE_2. This thesis is based on relatively wide MMW width region, 1700nm, to excite higher order mode TE_4 to improve performance of intersection and reduce size. That design is relatively more efficient than recent slot waveguide intersection. Furthermore it is a new trial using higher order mode, TE_4 mode in multimode-interference waveguide intersection structure.

2-2. Analysis method

Finite difference time domain (FDTD) method is using for analysis intersection design at 1550nm wavelength. Refractive index of silicon core is set as 3.476 and SiO_2 is 1.444 as cladding.

3. Analysis

3-1. Taper region analysis

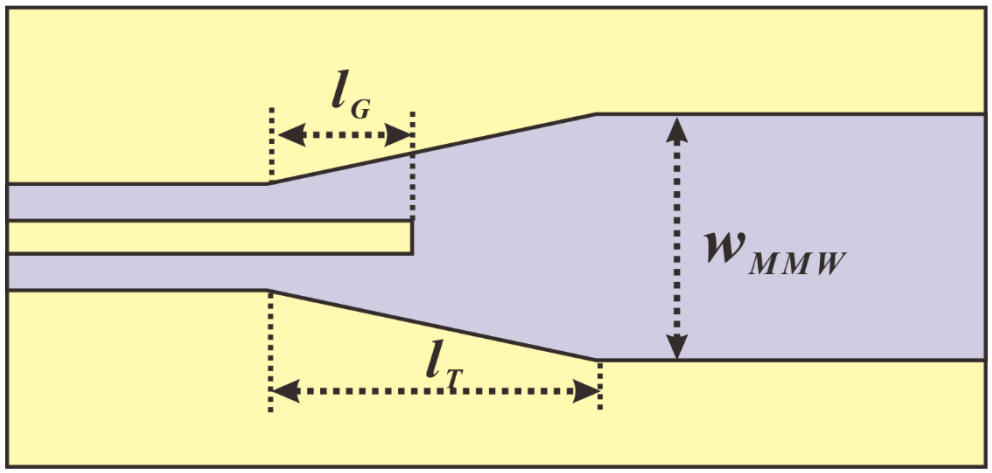

Fig. 3-1. A taper structure and parameters in taper region.

Fig. 3-1 shows taper structure and three key parameter of taper. Taper structure is determined by three parameter which are taper length, MMW width, and gap region length. Firstly, the length of taper influences to transmittance in taper structure. A short taper length results degradation of transmission due to loss of conversion in taper region. Therefore taper length have to be determined to enough long to reduce conversion loss in taper. A transmission of taper depending on taper length is depicted in Fig. 3-2. As shown in figure, transmission is relatively saturated over 3.0μm, taper length.

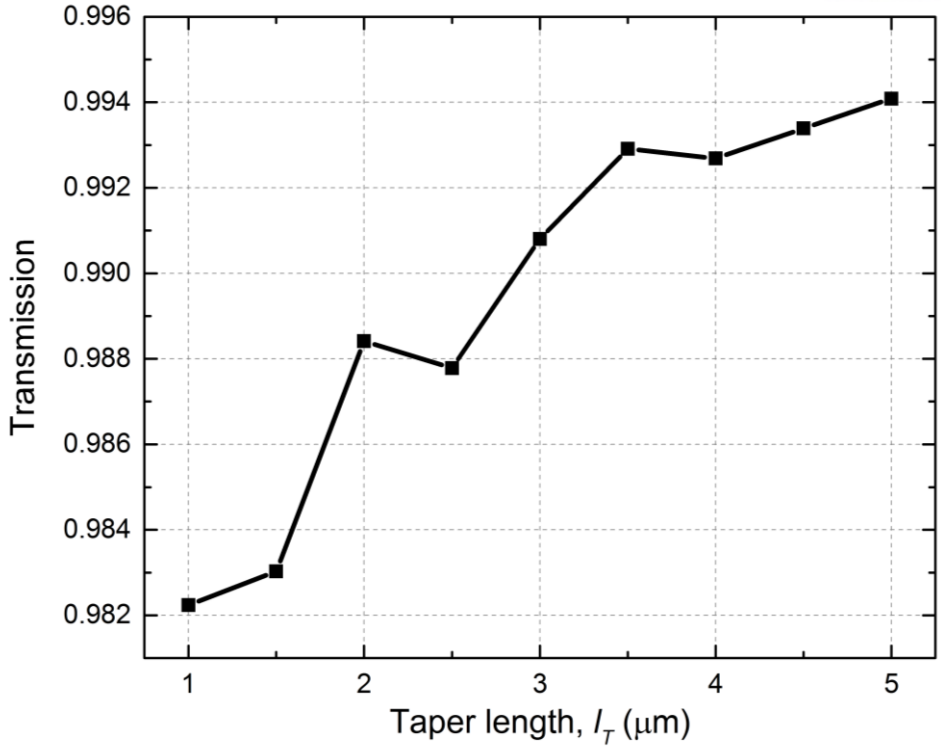

Fig. 3-2. Transmission of taper structure depending on taper length, l_T.

However there is tradeoff between transmission and size of structure. A device size is large if long taper length is selected.

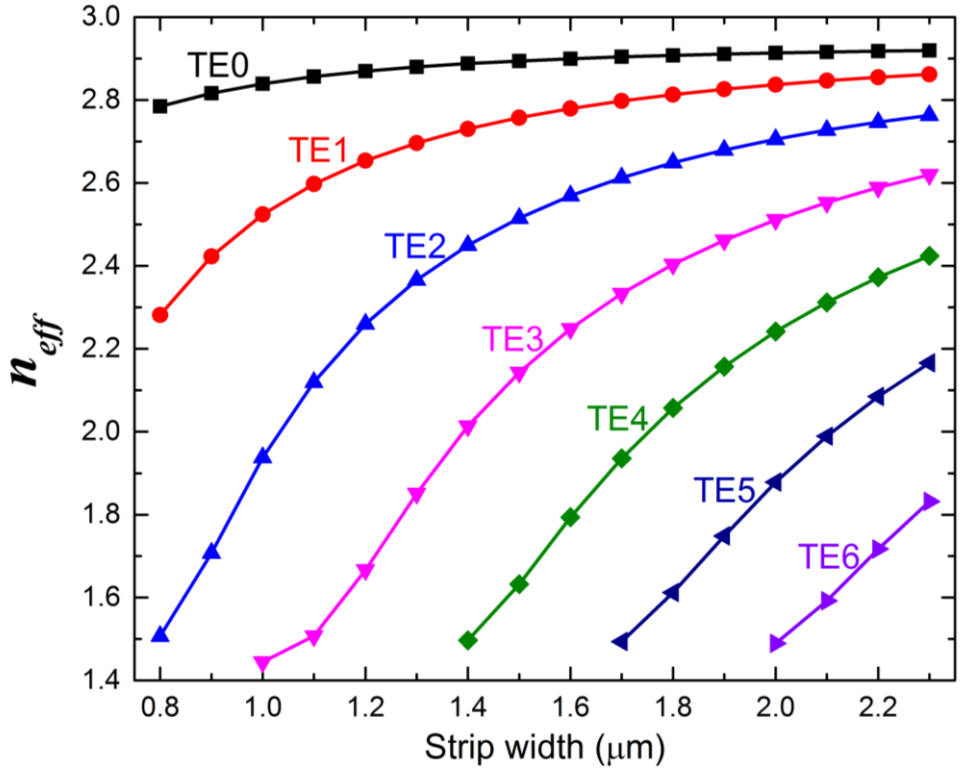

Fig. 3-3. Effective indices of modes in strip waveguide depending on strip width.

Fig. 3-3. shows effective indices of modes in multi-mode interference strip waveguide. Higher order lateral symmetric transverse electric mode, TE_2, exists when MMW width is larger than 0.8μm. Moreover next lateral symmetric mode, TE_4, appear when MMW width is larger than 1.4μm. Recent researches of slot waveguide intersection are based on MMW width as 1.2μm. These structures are only designed based on lateral symmetric fundamental two modes, TE_0 and TE_2 modes, in the multi-mode waveguide region. In this thesis, wider MMW width, 1.7μm, is selected to utilize higher order mode, TE_4, to enhance the performance of a slot waveguide intersection.

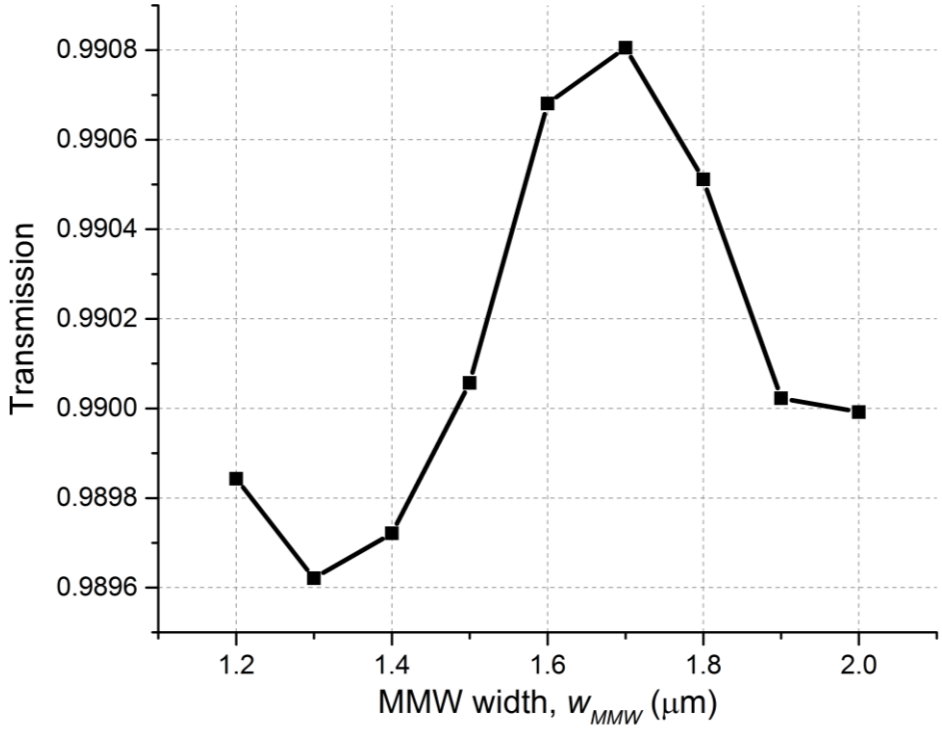

Fig. 3-4. A transmission of taper depending on multi-mode waveguide (MMW) width,w_{MMW}.

As shown in Fig. 3-4., the transmittance of the taper is increasing as enlarging MMW width for taper length 3.0μm taper structures. Transmittance is decreasing over 1.7μm due to increased power to radiation mode, TE_6. In the other words, guided light decreased from an increased radiative component.

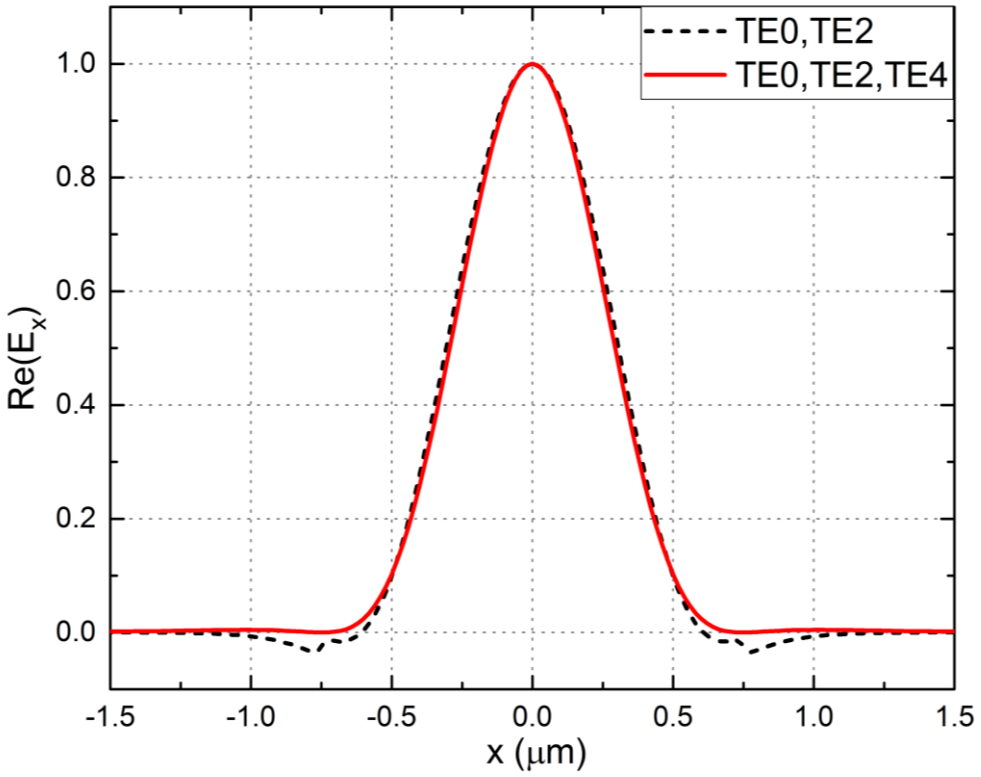

Fig. 3-5. A compariaion of E_x field at matching point in multi-mode waveguide.

Eelctric field plot from interference of TE0 and TE2 modes. (b) Normalized electric field plot from interference TE0, TE2, and TE4 modes. The black dot line of Fig. 3-6. represents field from two mode destructive interference of TE0 and TE2. The residual lateral component outside waveguide deters good performance of intersection. However by adding TE4 field component, the light shape is slightly more confined toward center and residual component outside waveguide is deterred. To make constructive interference between TE_0 and TE_4 modes.

TE_0 and TE_2 destructive position on propagation direction can be estimated by Eq. 3.1 equation with π phase difference between two modes. And constructive position of TE_0 and TE_4 can be derived by Eq. 3.2 and Eq. 3.3 equations with 2π and 4π phase shifts between TE_0 and TE_4 modes each other.

$$L_{\pi,0,2} = \frac{\pi - \Delta\Phi_{0,2}}{\beta_{TE0} - \beta_{TE2}}, \tag{3.1}$$

$$L_{2\pi,0,4} = \frac{2\pi - \Delta\Phi_{0,4}}{\beta_{TE0} - \beta_{TE4}}, \tag{3.2}$$

$$L_{4\pi,0,4} = \frac{4\pi - \Delta\Phi_{0,4}}{\beta_{TE0} - \beta_{TE4}}, \tag{3.3}$$

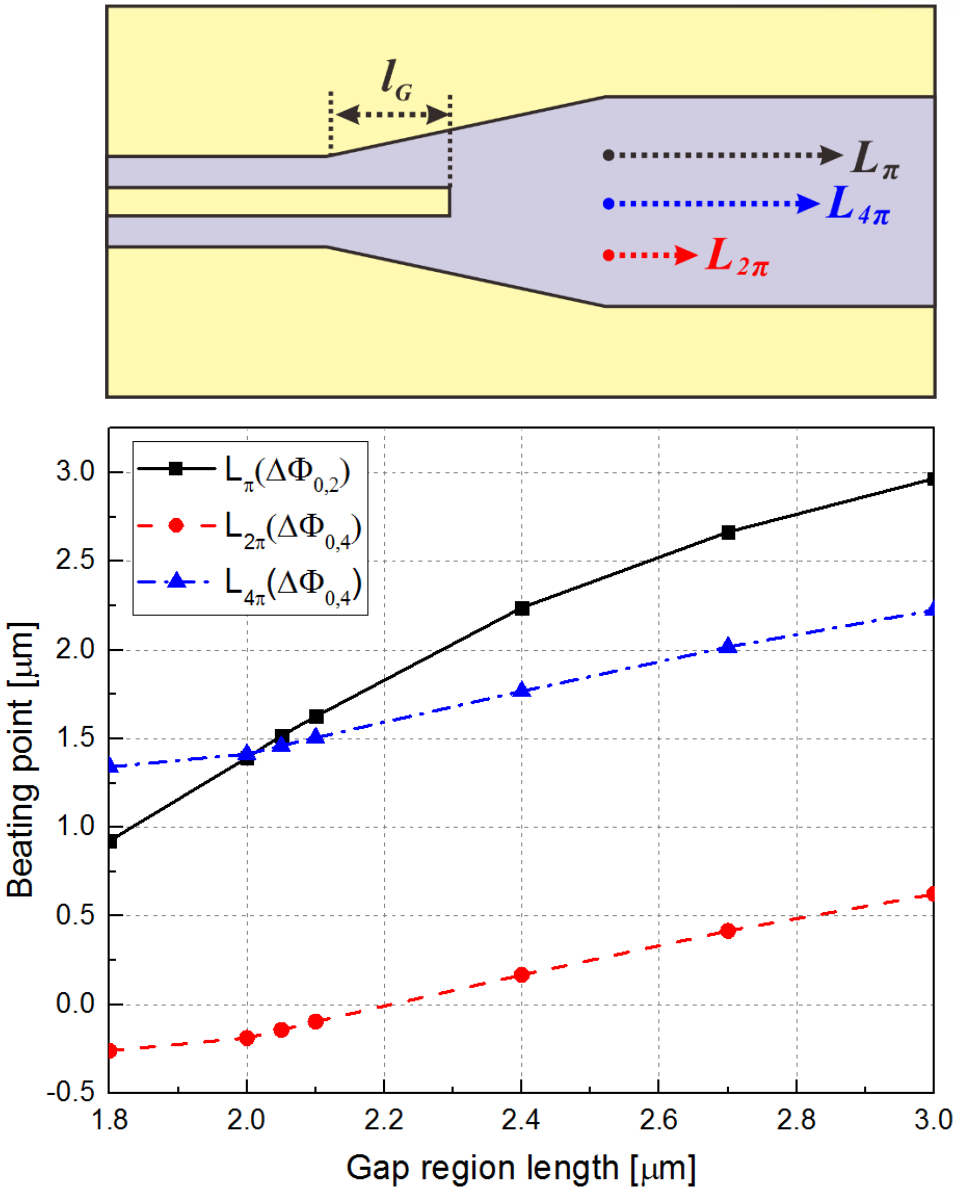

Fig. 3-6. A phase matching point in MMW. The black line is π phase shift position. Red and blue dot lines are 2π and 4π phase shift position respectively.

In the Fig. 3-6., black line shows a π phase difference position of TE_0 and TE_2. A red and blue dot lines displays 2 π, 4 π positions of TE_0 and TE_4. The beating length is defined a distance of multi-mode waveguide. Each position is matched when gap region length is 2.05μm. For that case, a π phase difference position of TE_0 and TE_2 is same as 2π phase difference position of TE_0 and TE_4. When light propagate with destructive interference between TE_0 and TE_2 modes, moreover with constructive interference between TE_0 and TE_4, the profile is more confined at the crossing center position. TE_4 component help the field profile more confined to lateral direction at MMW intersection center. Therefore device operates with enhanced through and suppressed crosstalk. By engineering gap region length, l_G, phase difference could be controlled. Furthermore beating length, L_π, also could be

determined. By selecting gap region length as matching point both $L_{\pi 0,2}$ and $L_{\pi 0,4}$, the TE_0 mode is influenced constructive interference from TE_2 mode and destructive interference from TE_4 mode. In summary, the beam profile is narrow and Gaussian-like beam profile at intersection center. That results good performance of intersection with low throughput and crosstalk.

3-2. Multi-mode interference region analysis

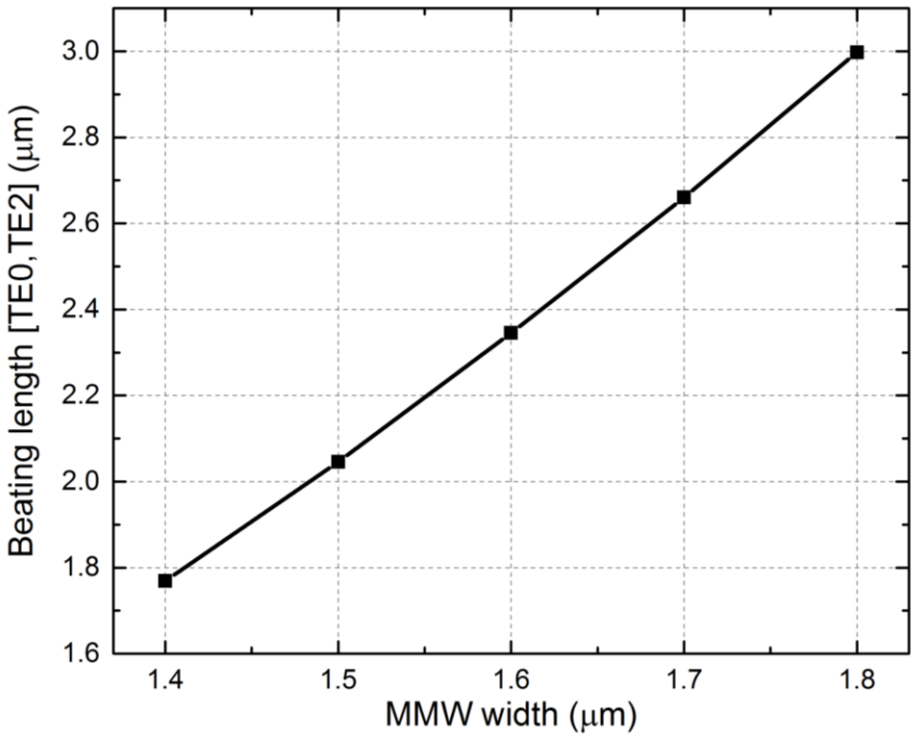

Fig. 3-7. The beating length depending on MMW width, w_{MMW}, derived by equation(3.4).

$$L_{MMW} = 2 \bullet L_{beat0,2} = \frac{2\pi}{\beta_{TE0} - \beta_{TE2}} = \frac{\lambda}{(n_{eff\ TE0} - n_{eff\ TE2})} \tag{3.4}$$

From the information of effective refractive indices of modes, the MMW length can be derived by Eq. 3.4. Fig. 3-7. shows calculated beating length of fundamental two lateral symmetric TE modes. Beating length increases as enlarging MMW width due to decreasing effective index difference between TE0 and TE2. As choosing wider MMW width, the total length of device is estimated as larger than the case of smaller MMW width. Furthermore accurate MMW length is can be achieved from Eq. 3.5 which is reflected phase difference.

$$L_{MMW} = 2 \bullet L_{beatlength} = 2 \bullet \frac{\pi - \Delta\Phi_{0,2}}{\beta_{TE0} - \beta_{TE2}} = \frac{\lambda(\pi - \Delta\Phi_{0,2})}{\pi(n_{eff\ TE0} - n_{eff\ TE2})} \tag{3.5}$$

3-3. Through, Crosstalk, and Reflection

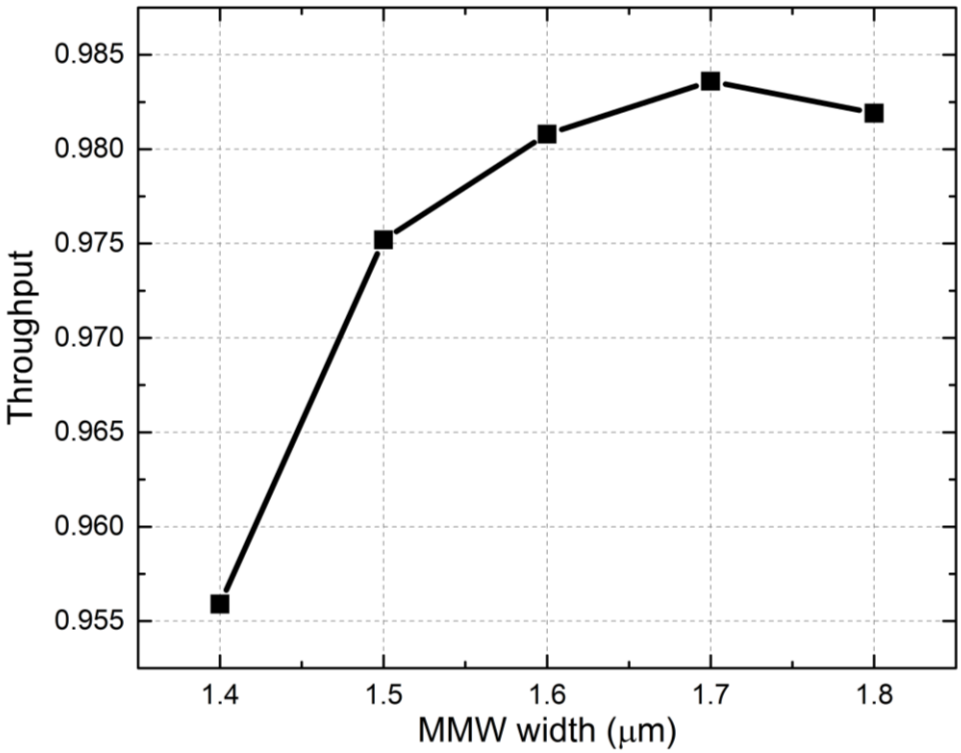

Fig. 3-8. The throughput depending on MMW width, w_{MMW},.

Fig. 3-8. shows throughput versus MMW width, as shown in a plot the through increases when MMW width increases from 1.4μm to 1.7μm range. For each value of w_{MMW}, l_T, and l_G are adjusted to make the throughput largest. Beyond 1.7μm range, the through decreases slightly. The reason of degradation is due to increased conversion component to radiation mode similar to TE_6 mode. Therefore the through of intersection decreases.

The normalized intensity profile and normalized transverse electric field profile are depicted in Fig. 3-9. As shown in Fig. 3-9. The light propagates through the proposed intersection structure with small distortion.

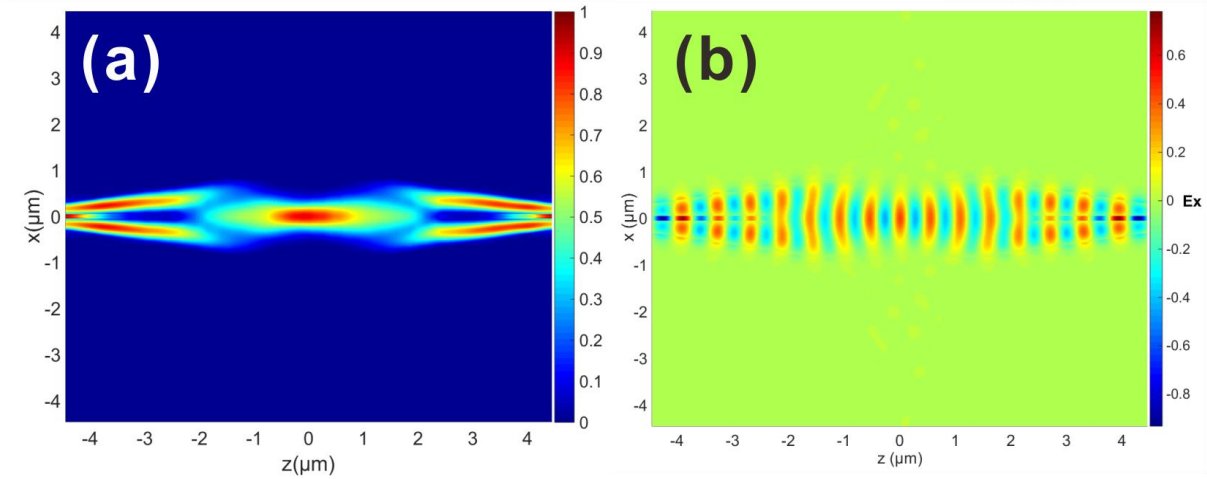

Fig. 3-9. (a) Normalized intensity profile (b) Normalized transverse electric field, E_x, profile.

3-4. Fabrication tolerance

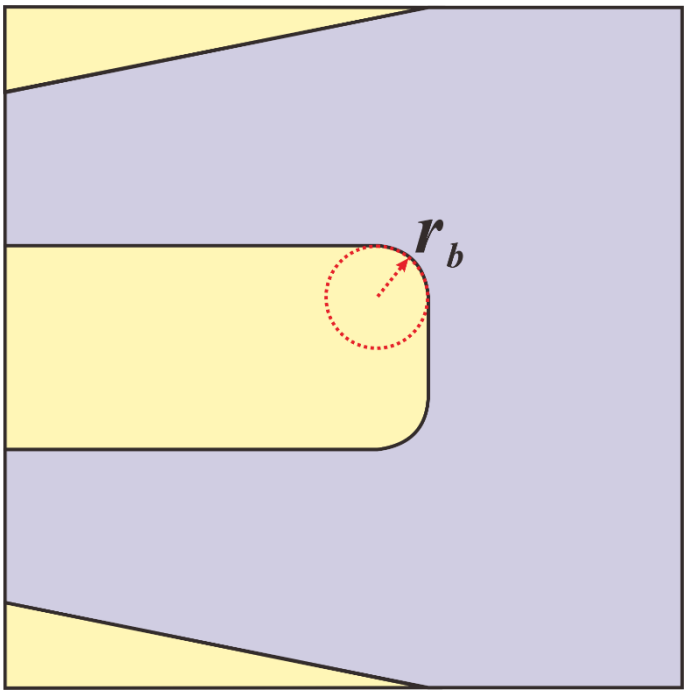

Fig. 3-10. A schematic diagram of blunt corners of slot region in taper structures.

In the fabrication process using e-beam lithography, it is avoidable to be blunted at the edge of slot region. To verify fabrication tolerance at the edge of slot region, round edge slot structure is applied at the end of slot in taper region.

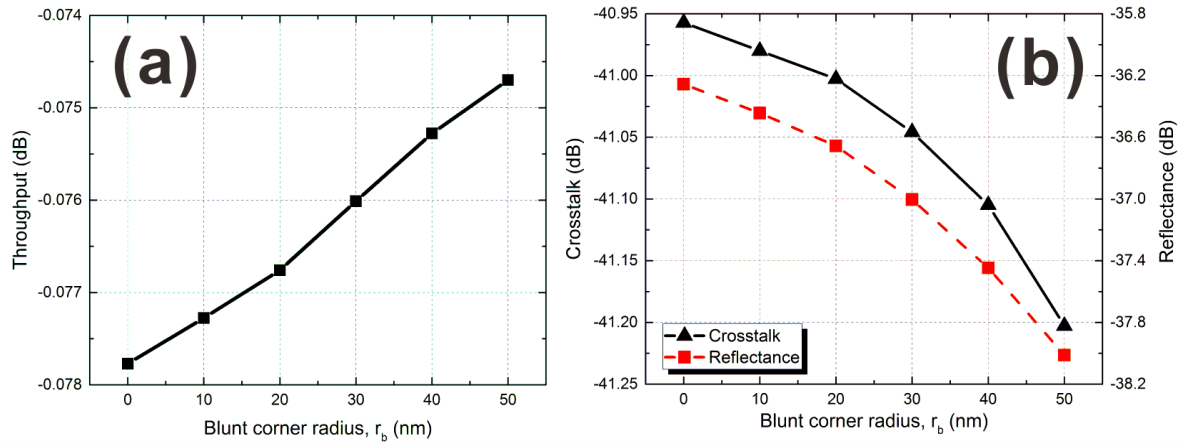

Fig. 3-11. (a) The throughput depending on blunt radius. (b) The crosstalk and reflection depending on blunt radius. The Black line is depicted crosstalk and red dot line shows reflection.

As shown in Fig. 3-11., throughput increases as enlarging blunt corner radius. Crosstalk and

reflectance decreases when blunt radius increases. The device performance is slightly enhanced for blunt corner. That enhancement comes from smooth change at the end of slot gap. On the contrary, slot waveguide intersection design based on sharp mode converter[5] has a problem for practical fabrication. It was reported that the blunt at sharp tip causes degradation of performance[15]. In this regard, the proposed structure has a merit for fabrication tolerance.

3-5. Wavelength dependency

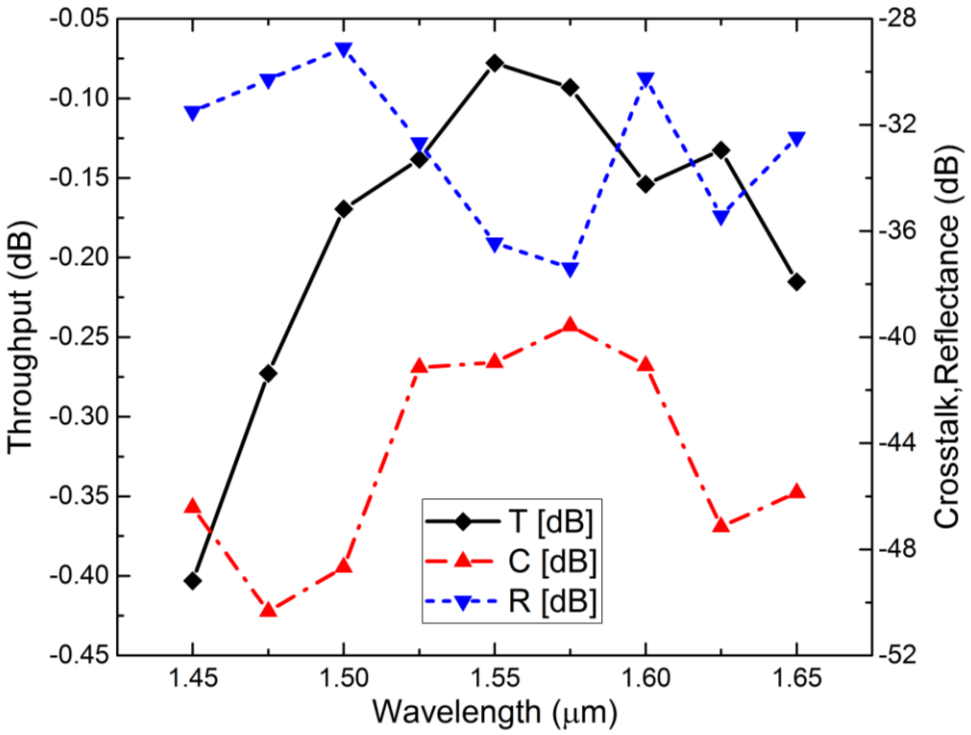

Fig. 3-12. Throughput, Crosstalk and Reflection depending on wavelength in the range from 1.45μm to 1.65μm.

Fig. 3-12. shows wavelength dependency of proposed device in the range from 1.45μm to 1.65μm. For 100nm bandwidth from 1.50μm to 1.60μm, the throughput is over -0.170dB. The crosstalk and reflection is under -36.6dB and -28.9dB respectively.

4. Conclusion

In conclusion, I proposed compact slot waveguide intersection based on multi-mode interference waveguide. I verified using finite difference time domain method (FDTD, Lumerical) at 1550nm wavelength. The device throughput, crosstalk and reflection is -0.078dB, -41dB, and reflection, -36dB. The total device size is $(8.9\mu m)^2$. Different from recently reported designs, we choose wider multi-mode waveguide width as 1700nm. TE_4 mode in multi-mode waveguide results a narrower beam shape in lateral direction. As a result, more efficient intersection structure could be achieved. Moreover, device size is 33% smaller than a reported design[5]. For 100nm bandwidth from 1.50μm to 1.60μm, the throughput is over -0.170dB. The crosstalk and reflection is under -36.6dB and -28.9dB respectively. Proposed structure is strong for fabrication tolerance. The performance is slightly enhanced for blunt corner.

Proposed slot waveguide intersection structure could be a component of cascade switch matrix based on slot ring resonator. Slot ring resonators can be utilized to efficient modulation. The reason is that there is a very high electric field at low index region in a slot waveguide. By placing electro optical polymer in low index region, fast and efficient modulation can be achieved. To efficient coupling between a slot ring resonator and bus waveguide, slot waveguide intersections are essential components. Recently reported fabricated very high-Q factor slot ring resonators shows prospect of a switch matrix based on slot ring resonator. Furthermore more improved performance of proposed design could be possible by adapting logarithmical taper structure to reduce conversion loss in transition region.

REFERENCES

1. D. A. B. Miller, "Device Requirements for Optical Interconnects to Silicon Chips," in *Proceedings of the IEEE*, vol. 97, no. 7, pp. 1166-1185, July 2009.

2. A. W. Poon, X. Luo, F. Xu and H. Chen, "Cascaded Microresonator-Based Matrix Switch for Silicon On-Chip Optical Interconnection," in *Proceedings of the IEEE*, vol. 97, no. 7, pp. 1216-1238, July 2009.

3. T. Baehr-Jones, M. Hochberg, G. Wang, R. Lawson, Y. Liao, P. A. Sullivan, L. Dalton, A. K. J. Jen, A. Scherer, "Optical modulation and detection in slotted silicon waveguides," *Opt. Exp*., vol. 13, no. 14, Jul. 2005.

4. Y. Xu, J. Wang, J. Xiao and X. Sun, "Design of a compact silicon-based slot-waveguide crossing composed of an orthogonal strip multimode waveguide and four logarithmical mode converters," *J. Phy. D*, Vol. 46, pp. 455102, Oct. 2013.

5. Y. Xu, J. Wang, J. Xiao, X. Sun, "Design of a compact silicon-based slot-waveguide crossing," *Appl. Opt.*, vol. 52, no. 16, pp. 3737-3744, Jun. 2013.

6. T. Fukazawa, T. Hirano, F. Ohno, and T. Baba, "Low loss intersection of Si photonic wire waveguides," *Jpn. J. Appl. Phys.*, vol. 43, no. 2, pt. 1, pp. 646–647, Feb. 2004.

7. L. B. Soldano and E. C. M. Pennings, "Optical multi-mode interference devices based on self-imaging: principles and applications," in Journal of Lightwave Technology, vol. 13, no. 4, pp. 615-627, Apr 1995.

8. V. R. Almeida, Q. Xu, C. A. Barrios, and M. Lipson, "Guiding and confining light in void nanostructure," Opt. Lett. vol. 29, pp. 1209-1211, Jan. 2004.

9. S. Serna, W. Zhang, X. Leroux, D. Gao, D. Zhang, L. Vivien, and E. Cassan, "Potential for large optical gain improvement of erbium-doped slot waveguide amplifiers in silicon photonics," *J. Opt. Soc. Am. B*, vol. 31, pp. 2021-2028, Sep. 2014.

10. T. Baehr-Jones, B. Penkov, J. Huang, P. Sullivan, J. Davies, J. Takayesu, J. Luo, T. D. Kim, L. Dalton, A. Jen, M. Hochberg, A. Scherer, "Nonlinear polymer-clad silicon slot waveguide modulator

with a half wave voltage of 0.25 V", *Appl. Phys. Lett.*, vol. 92, pp. 163303, 2008.

11. T. Fujisawa and M. Koshiba, "Theoretical investigation of ultrasmall polarization-insensitive 1 ×2 multimode interference waveguides based on sandwiched structures," in *IEEE Photon. Technol. Lett.*, vol. 18, no. 11, pp. 1246-1248, June 2006.

12. W. Zhang, S. Serna, X. L. Roux, C. Alonso-Ramos, L. Vivien, and E. Cassan, "Analysis of silicon-on-insulator slot waveguide ring resonators targeting high Q-factors," *Opt. Lett.* vol. 40, pp. 5566-5569, Dec. 2015.

13. T. Claes, J. Girones Molera, K. De Vos, E. Schacht, R. Baets and P. Bienstman, "Label-Free Biosensing With a Slot-Waveguide-Based Ring Resonator in Silicon on Insulator," in *IEEE Photonics Journal*, vol. 1, no. 3, pp. 197-204, Sept. 2009.

14. F. Li, X. Sun, J. Wu, X. Hu, L. Zhou and Y. Su, "Efficient Fiber-to-Slot-Waveguide Grating Couplers Based on a Double-Strip Waveguide," in *IEEE Photonics Technology Letters*, vol. 25, no. 23, pp. 2377-2380, Dec.1, 2013.

15. Z. Wang, N. Zhu, Y. Tang, L. Wosinski, D. Dai, and S. He, "Ultracompact low-loss coupler between strip and slot waveguides," *Opt. Lett*. vol. 34, pp. 1498-1500, May 2009.